α-Ga$_2$O$_3$ grown by low temperature atomic layer deposition on sapphire

J.W. Roberts[a], J.C. Jarman[b], D.N. Johnstone[b], P.A. Midgley[b], P.R. Chalker[a], R.A. Oliver[b], F.C-P. Massabuau[b*]

[a] *School of Engineering, The University of Liverpool, Brownlow Hill, Liverpool L69 3GH, UK*

[b] *Department of Materials Science and Metallurgy, University of Cambridge, 27 Charles Babbage Road, Cambridge CB3 0FS, UK*

* Email: fm350@cam.ac.uk

Abstract

α-Ga$_2$O$_3$ is a metastable phase of Ga$_2$O$_3$ of interest for wide bandgap engineering since it is isostructural with α-In$_2$O$_3$ and α-Al$_2$O$_3$. α-Ga$_2$O$_3$ is generally synthesised under high pressure (several GPa) or relatively high temperature (~500°C). In this study, we report the growth of α-Ga$_2$O$_3$ by low temperature atomic layer deposition (ALD) on sapphire substrate. The film was grown at a rate of 0.48 Å/cycle, and predominantly consists of α-Ga$_2$O$_3$ in the form of (0001)-oriented columns originating from the interface with the substrate. Some inclusions were also present, typically at the tips of the α-phase columns and most likely comprising ε-Ga$_2$O$_3$. The remainder of the Ga$_2$O$_3$ film – *i.e.* nearer the surface and between the α-Ga$_2$O$_3$ columns, was amorphous. The film was found to be highly resistive, as is expected for undoped material. This study demonstrates that α-Ga$_2$O$_3$ films can be grown by low temperature ALD and suggests the possibility of a new range of ultraviolet optoelectronic and power devices grown by ALD. The study also shows that scanning electron diffraction is a powerful technique to identify the different polymorphs of Ga$_2$O$_3$ present in multiphase samples.

Keywords

B2. Semiconducting gallium compounds, B1. Oxides, A3. Atomic layer epitaxy, A1. X-ray diffraction, A1. Scanning electron diffraction.

1. Introduction

Ga$_2$O$_3$ has received attention as a wide band gap semiconductor with potential applications in electronics and optics [1]. Bandgap engineering is required to construct various optoelectronic devices, and polymorphic control is required to achieve the necessary variation in composition in ternary and quaternary group III-oxides. Ga$_2$O$_3$ adopts numerous polymorphs and complete understanding of

polymorphism in this system remains lacking [2,3]. High-quality structures are known for rhombohedral α [4], monoclinic β [5], cubic γ [6], and hexagonal ε [2] polymorphs, all of which are based on approximately hexagonally close-packed layers of oxygen ions with gallium ions occupying the octahedral and tetrahedral sites differently [2]. Two further polymorphs have been suggested, namely δ [6] and orthorhombic κ [2,3], the latter being related to the ε phase as an ordered variant. The thermodynamically stable polymorph under standard conditions is the monoclinic β phase (space group 12, C2/m), which has consequently been the focus of most research efforts [7]. In the context of band gap engineering however, it has been suggested that rhombohedral α-Ga_2O_3 (space group 167, R$\bar{3}$c) is desirable [8] since Al_2O_3 and In_2O_3 can both be found in isostructural polymorphs – α-Al_2O_3 is thermodynamically stable corundum while α-In_2O_3 is metastable [9]. With a band gap ranging from 3.8 eV (α-In_2O_3 [8]) to 8.8 eV (α-Al_2O_3 [10]), controlling the growth of α-phase group III-oxides could pave the way for a number of ultraviolet optoelectronics and power devices.

α-Ga_2O_3 has traditionally been synthesised under high pressures of several GPa [11,12]. More recently several studies have reported the growth of α-Ga_2O_3 at temperatures near 500 °C using mist chemical vapor deposition (mist-CVD) [8], molecular beam epitaxy (MBE) [13] and halide vapor phase epitaxy (HVPE) [14]. Schewski *et al.* also observed the growth of up to 3 monolayers of α-Ga_2O_3 by metalorganic vapor phase epitaxy (MOVPE) at 850 °C, pulsed-laser deposition (PLD) at 650 °C or MBE at 675 °C, beyond which the film adopted the β phase [15]. However, to date there are no reports of α-Ga_2O_3 grown by atomic layer deposition (ALD). Previous studies using ALD to deposit Ga_2O_3 have resulted in an amorphous film [16-21] that eventually crystallized into β-Ga_2O_3 upon post-growth annealing. In the present study, we have achieved the growth of the metastable phase α-Ga_2O_3 using ALD. Owing to a similar crystal structure and low lattice mismatch (around 4.8%) with α-Ga_2O_3, sapphire (α-Al_2O_3) was chosen for substrate since it may allow one to overcome the thermodynamic instability of α-Ga_2O_3.

2. Methods

Deposition of Ga_2O_3 was achieved using alternating pulses of triethylgallium (TEGa) and O_2 plasma in an Oxford Instruments Plasma-OpAL ALD system. A *c*-plane sapphire substrate with a miscut of 0.25±0.10° towards (11$\bar{2}$0) was employed. The substrate temperature was set at 250 °C, reactor wall temperatures were at 150 °C, the TEGa bubbler was kept at ~25 °C and the delivery lines from the TEGa bubbler to the deposition chamber were set at 50 °C. Each ALD cycle consisted of one 0.1 s pulse of TEGa with 100 sccm of Ar carrier gas, a 5 s purge using 100 sccm Ar through the TEGa line, a 5 s, 300 W O_2 plasma using 20 sccm O_2, and finally a 5 s purge using 100 sccm Ar. 2730 cycles were performed. The substrates were left at growth temperature and under vacuum for approximately 4 hours before being removed and cooled. ALD process parameters were chosen based on work by

Shih *et al.*, where they demonstrated saturative ALD growth of Ga_2O_3 from TEGa and O_2 plasma. TEGa dose times above 0.1 s and O_2 plasma times above 5 s were found to produce no increase in the Ga_2O_3 growth rate [17]. Furthermore, a wide ALD growth window has been reported between 100°C and 400°C when using TEGa and O_2 plasma for the growth of Ga_2O_3 [18]. Several films have been grown in separate growth runs using the same growth parameters. X-ray diffraction characterisation of these films was identical to that presented hereafter, thus demonstrating the repeatability of the growth process. Post-deposition film thickness measurements were made by ellipsometry using a Horiba Jobin Yvon MM-16 Spectroscopic Ellipsometer and fitted to a Ga_2O_3 Cauchy model using a wavelength range of 430-850 nm. Ellipsometry results showed a deposition of ~130 nm giving a growth rate of 0.48 Å/cycle (with an estimated error of ~10% for both the thickness and growth rate). X-ray diffraction (XRD) was used to assess the crystallite size, texture and quality in the deposited films. XRD was carried out on a PANalytical Empyrean diffractometer with a Cu $K_{\alpha1}$ X-ray source (λ = 1.5405974 Å [22]), a hybrid monochromator, and either a two-bounce Ge crystal analyzer (for 2θ-ω and ω scans) or a PIXcel detector (for reciprocal space maps (RSMs)). (Scanning) transmission electron microscopy ((S)TEM) was performed on samples prepared in cross-section by standard mechanical polishing using diamond lapping films, followed by Ar^+ ion milling at 5 kV until a hole was visible and polishing from 1 kV down to 0.1 kV. A Tecnai F20 operated at 200 kV was used for annular dark-field STEM (ADF-STEM) imaging, while a JEOL 4000EX operated at 400 kV was employed for high-resolution TEM (HR-TEM) imaging. Scanning electron diffraction (SED), which involves the acquisition of an electron diffraction pattern at each probe position [23] as a convergent electron probe is scanned across the sample, was performed using a Philips CM300 operated at 300 kV and retrofitted with a NanoMegas Digistar system. This system enables the simultaneous scan and acquisition of diffraction patterns with an external optical charge coupled device imaging the phosphor viewing screen of the microscope. In this way, nanobeam electron diffraction pattern (with ~2 mrad convergence angle) were acquired with a step size of ~2.5 nm and a camera length of 210 mm. The SED data was inspected and analysed using a Python library for crystallographic electron microscopy [24,25]. The diffraction patterns were first corrected for geometric distortions resulting from the off-axis camera geometry by application of an affine transformation. A series of diffraction contrast images were then formed by plotting the intensity within a selected subset of pixels in the diffraction pattern as a function of probe position to form so-called 'virtual dark-field' (VDF) images. Here, circular integration windows with a 2 pixel radius were used to form such images.
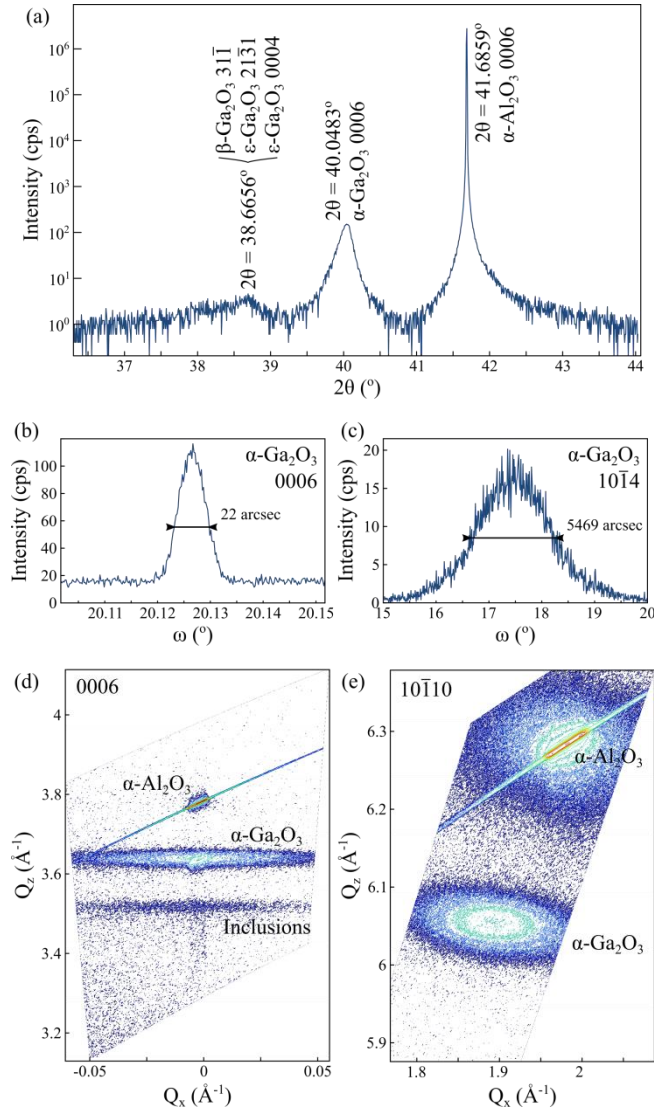
3. Results

Figure 1. (a) 2θ-ω scan recorded around the α-Al$_2$O$_3$ 0006 reflection. (b-c) Rocking curve ω scans recorded on the (b) α-Ga$_2$O$_3$ 0006 and (c) α-Ga$_2$O$_3$ 10$\bar{1}$4 reflections. (d-e) RSMs around the (d) α-Al$_2$O$_3$ 0006 and (e) α-Al$_2$O$_3$ 10$\bar{1}$10 reflections.

A 2θ-ω scan taken around the α-Al$_2$O$_3$ 0006 reflection is shown in Figure 1(a). Alongside the substrate peak at 2θ = 41.6859°, a peak can be clearly observed at 2θ = 40.0483°, corresponding to the α-Ga$_2$O$_3$ 0006 reflection. Since other known polymorphs of Ga$_2$O$_3$ do not diffract in this range, this is clear evidence that the deposited film is α-Ga$_2$O$_3$. We note that only one peak corresponding to the α-Ga$_2$O$_3$ 0006 reflection was visible in the texture map (not shown here), indicating that the α-Ga$_2$O$_3$ crystal is oriented with the [0001] direction parallel to the [0001] direction of the sapphire substrate. Considering the atomic structure, this corresponds to alignment of the oxygen layers in both structures, which is perhaps to be expected. This suggests that the sapphire substrate played a critical role in determining the phase and orientation of the film. An estimate of the size of the α-Ga$_2$O$_3$ crystallites can be obtained using the Scherrer equation: τ = Kλ/Bcosθ, where τ is the mean size of the crystallites, K a constant assumed close to 0.9, λ the wavelength of incoming X-rays, B the full-width at half-

maximum (FWHM) of the peak (after removal of the instrumental broadening), and θ the Bragg angle. The data indicate that the film consists of α-Ga_2O_3 crystallites of about 50-60 nm in size. An additional weak peak can be distinguished at lower 2θ values, which could be attributed to one or several of the following reflections: β-Ga_2O_3 $31\bar{1}$, ε-Ga_2O_3 0004 or ε-Ga_2O_3 $21\bar{3}1$, and indicates the presence of inclusions in the dominantly (0001)-oriented α-Ga_2O_3 film. Since ε-Ga_2O_3 0004 also corresponds to the oxygen layers in this structure, it may be expected that the alignment of such planes continues and that this is likely to be the correct assignment, although this can only be tentative.

The crystalline quality of the film can be assessed by measuring the FWHM of rocking curve ω scans taken on symmetric and skew-symmetric reflections. The combination of these two measurements gives information about the tilt and twist of crystals within the film, respectively. Here we used the 0006 and $10\bar{1}4$ reflections, as illustrated in Figure 1(b-c). The rocking curve on the 0006 reflection has a FWHM of 22 arcsec, which is in line with values reported in the literature for α-Ga_2O_3 grown by mist-CVD [26,27]. This value indicates an excellent film quality, as far as the tilt of the crystals is concerned. However, we also note a "background" signal at about 15 cps on the ω-scan, possibly indicating that the film may contain a region with much lower crystalline quality. The rocking curve on the $10\bar{1}4$ reflection is much broader, with a FWHM of 5469 arcsec. On mist-CVD-grown films, Fujita *et al.* also reported a very broad $10\bar{1}4$ reflection [26]. This indicates there is some amount of twist of the α-Ga_2O_3 crystals around the [0001] direction. If we were to interpret these results in terms of dislocation type and density, we would say that there is a predominance of dislocations with Burgers vectors containing an a-component as opposed to a c-component. However, further structural analysis by TEM is required for a more appropriate interpretation of this twist.

To assess the strain state of the film, RSMs were recorded around the symmetric 0006 and asymmetric $10\bar{1}10$ reflections. We can at first notice that the α-Ga_2O_3 $10\bar{1}10$ reflection does not lie at the same Q_x position as the α-Al_2O_3 $10\bar{1}10$ reflection, and hence has a different in-plane lattice parameter, indicating that the α-Ga_2O_3 is partially relaxed on the α-Al_2O_3 substrate. By measuring the peak positions, we obtained lattice parameters for α-Ga_2O_3 of a = 4.9449 Å and c = 13.4976 Å, which, taking values for relaxed α-Ga_2O_3 of a = 4.9825 Å [26,28], yields an 83±9% relaxation of the film relative to the substrate.

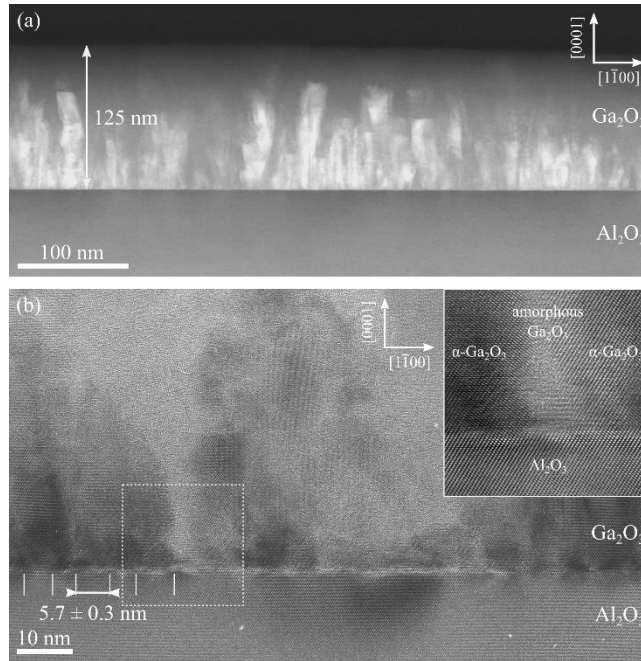**Figure 2.** (a) ADF-STEM and (b) HR-TEM image of the sample observed along the α-Al$_2$O$_3$ ⟨11$\bar{2}$0⟩ zone-axis. In inset, ABSF-filtered (average background subtraction filter) image of the interface region indicated with a square in (b).

The sub-surface structure of the sample was inspected by cross-sectional (S)TEM. As can be seen in Figure 2(a) by ADF-STEM, the Ga$_2$O$_3$ film has a columnar structure. The contrast in ADF-STEM being a combination of Z-contrast and diffraction contrast, it appears that the bright columns correspond to the α-Ga$_2$O$_3$ crystals separated by presumably amorphous Ga$_2$O$_3$ in grey. The film thickness measured from the ADF-STEM image is ~125 nm which is consistent with the value obtained via ellipsometry. The ADF-STEM image illustrates the relatively large spread in column height and width. We measured column heights ranging from 27 nm up to the full thickness of the film (125 nm), with average height value of 72 ± 8 nm in good agreement with the value obtained from Scherrer analysis of the XRD data. The thickness of the columns ranges from as little as 2 nm to 23 nm, with an average value of 9 ± 2 nm. An HR-TEM image of the film, taken along the ⟨11$\bar{2}$0⟩ zone-axis, is shown in Figure 2(b), and confirms that the crystallographic orientation relationship between the α-Ga$_2$O$_3$ columns and α-Al$_2$O$_3$ substrate is locally close to $[11\bar{2}0]_{Ga_2O_3}$ || $[11\bar{2}0]_{Al_2O_3}$, $(0001)_{Ga_2O_3}$ || $(0001)_{Al_2O_3}$, consistent with XRD results. The α-Ga$_2$O$_3$ crystals are also separated by amorphous material (see inset of Figure 2(b)). The columns can be seen to originate from the interface with the substrate, emphasizing again the role played by the sapphire substrate in stabilizing the α phase. Periodic variations in contrast at the substrate/film interface can also be observed, as illustrated in Figure 2(b), and indicate the presence of misfit dislocations. We note a regular spacing of the dislocations of 5.7±0.3 nm. While this cannot be interpreted quantitatively as a measure of strain relaxation given the non-planar growth of the α-Ga$_2$O$_3$ crystals (if the film were planar, a dislocation

spacing of 9.1 nm would suffice to completely relax the film as $21 \, d_{1\bar{1}00}^{\alpha-Ga_2O_3} = 22 \, d_{1\bar{1}00}^{\alpha-Al_2O_3} = 9.1$ nm), it supports our XRD results that the α-Ga₂O₃ crystals are largely relaxed.
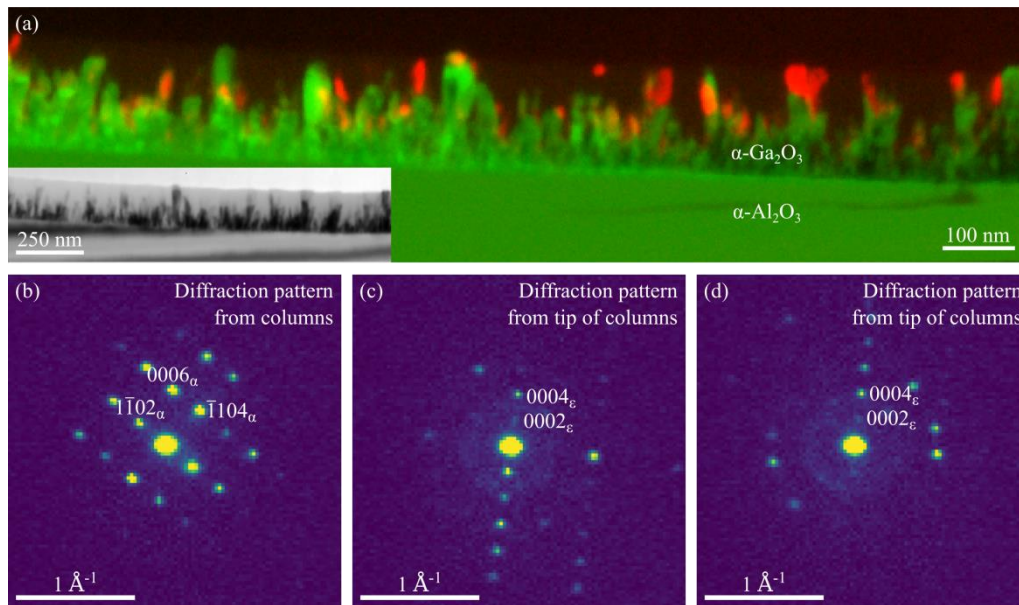
Figure 3. SED of the Ga₂O₃ film observed near the α-Al₂O₃ ⟨11$\bar{2}$0⟩ zone-axis. (a) Composite diffraction contrast image formed plotting the intensity of selected reflections as a function of probe position. Green corresponds to reflections in the α-Ga₂O₃ ⟨11$\bar{2}$0⟩ zone-axis pattern and red corresponds to additional reflections identified in the data. Inset shows the intensity of the direct beam revealing the full extent of the film including non-diffracting components. Representative diffraction patterns (b) from the α-Ga₂O₃ columns, (c-d) from the tips which are most likely ε-Ga₂O₃.

The local atomic structure across a region of the deposited film was assessed using SED, as shown in Figure 3. VDF images were formed using numerous reflections and combined as a colour composite image to reveal the location of the oxide phases. Intensity from reflections present in the α-Ga₂O₃ ⟨11$\bar{2}$0⟩ zone-axis pattern (see Figure 3(b)) is shown in green in Figure 3(a) and intensity from reflections not in this pattern, mostly corresponding to other polymorphs, is shown in red. This verifies that the film is predominantly columnar α-Ga₂O₃ and that only the α-phase is observed within ~50 nm of the substrate. These α-Ga₂O₃ columns are also oriented near to the orientation of the α-Al₂O₃ substrate throughout their extent. A more quantitative assessment of the local orientation of the α-Ga₂O₃ was made by performing an orientation mapping over the region near to the substrate based on matching simulated templates for all orientations with each diffraction pattern [29], which revealed orientation variations within ±4°, consistent with the broadening of the α-Ga₂O₃ 10$\bar{1}$4 reflection in XRD. Other polymorphs are present at the tips of the α-Ga₂O₃ columns and there is a significant amorphous component to the film, which does not diffract strongly. Representative diffraction patterns from the second phase inclusions are shown in Figure 3(c-d). These patterns illustrate that a characteristic feature of diffraction from these regions is the presence of reflections with g-vectors approximately half the length of the 0006_α g-vector. These reflections may be attributed to the 0002_ε

reflection, with the 0004_ε then being approximately coincident with the 0006_α and corresponding to the hexagonally close-packed oxygen layers in each structure. This corroborates the suggestion that the primary inclusion phase in the film is ε-phase with close-packed oxygen layers remaining aligned between phases. Given that both phases share a common hexagonally close-packed oxygen layer, it is possible that, during growth, the tip of the crystalline α-Ga_2O_3 columns provides suitable nucleation sites for ε-Ga_2O_3. The transition from the α phase to the ε phase is not unexpected, owing that the latter has a lower formation energy according to first principle calculations [30]. It should be noted, that in the regions near to the column tips diffraction patterns were often recorded containing reflections from multiple crystals and therefore unambiguous indexation of these patterns was not generally possible.

The film was tested for electrical properties. Ti/Au contacts of dimensions 200 μm x 400 μm and 10/80 nm in thickness were deposited by thermal evaporation and lift-off. Electrical testing showed that the sample is highly resistive, with a resistance approaching 5 x10^{10} Ω measured between two contacts spaced 5 μm apart. The resistance was so high that reliable measurement could not be made between wider spaced contacts precluding determination of a resistivity value for the deposited material. High values of resistance for undoped α-Ga_2O_3 films have also been reported in the literature, and were found to reduce significantly upon Sn-doping [31,32]. The high resistance measured here could also be compounded by the multiple phase structure of the film.

4. Conclusion

In conclusion, we have demonstrated that α-Ga_2O_3 can be deposited by low temperature ALD on *c*-plane sapphire substrate. The film was grown at a rate of 0.48 Å/cycle. We found that the film thus grown consists of (0001)-oriented α-Ga_2O_3 columns originating from the substrate. Some inclusions, most likely of the ε phase were also observed primarily at the tip of the columns, and amorphous phase was found located nearer the surface of the film and between the α-Ga_2O_3 columns. It is anticipated that with further improvement of the crystallinity and electrical properties of the film, this study opens the path for a new range of semiconductor devices that could be produced by ALD.

Acknowledgements

References

[1]   M. Higashiwaki, K. Sasaki, H. Murakami, Y. Kumagai, A. Koukitu, A. Kuramata, T. Masui, and S. Yamakoshi, Semicond. Sci. Technol. **31**, 34001 (2016)

[2]   H.Y. Playford, A.C. Hannon, E.R. Barney, and R.I. Walton, Chem. Eur. J. **19**, 2803-2813 (2013)

[3]   I. Cora, F. Mezzadri, F. Boschi, M. Bosi, M. Caplovicova, G. Calestani, I. Dodony, B. Pecz, R. Fornari, Cryst. Eng. Comm. **19**, 1509-1516 (2017)

[4]   I. Levin and D. Brandon, J. Am. Ceram. Soc. **81**, 1995-2012 (1998)

[5]   S. Geller, J. Solid State Chem. **20**, 209-210 (1977)

[6]   R. Roy, V.G. Hill, and E.F. Osborn, J. Am. Chem. Soc. **74**, pp 719-722 (1952)

[7]   S.I. Stepanov, V.I. Nikolaev, V.E. Bougrov, and A.E. Romanov, Rev. Adv. Mater. Sci. **44**, 63-86 (2016)

[8]   S. Fujita, and K. Kaneko, J. Cryst. Growth **401**, 588-592 (2014)

[9]   S.Z. Karazhanov, P. Ravindran, P. Vajeeston, A. Ulyashin, T. G. Finstad, and H. Fjellvåg, Phys. Rev. B **76**, 075129 (2007)

[10]   R.H. French, J. Am. Ceram. Soc. **73**, pp 477-489 (1990)

[11]   J.P. Remeika, and M. Marezio, Appl, Phys. Lett. **8**, 87-88 (1966)

[12]   D. Machon, P.F. McMillan, B. Xu, and J. Dong, Phys. Rev. B **73**, 094125 (2006)

[13]   R. Kumaran, T. Tiedje, S.E. Webster, S. Penson, and W. Li, Optics Letters **35**, 3793-3795 (2010)

[14]   Y. Oshima, E.G. Víllora, and K. Shimamura, Appl. Phys. Express **8**, 055501 (2015)

[15]   R. Schewski, G. Wagner, M. Baldini, D. Gogova, Z. Galazka, T. Schulz, T. Remmele, T. Markurt, H. von Wenckstern, M. Grundmann, O. Bierwagen, P. Vogt, and M. Albrecht, Appl. Phys. Express **8**, 011101 (2015)

[16]   D.J. Comstock, and J.W. Elam, Chem. Mater. **24**, 4011-4018 (2012)

[17]   H.-Y. Shih, F.-C. Chu, A. Das, C.-Y. Lee, M.-J. Chen, and R.-M. Lin, Nanoscale Research Letters **11**, 235 (2016)

[18]   I. Donmez, C. Ozgit-Akgun, and N. Biyikli, J. Vac. Sci. Technol. A **31**, 01A110 (2013)

[19]   D.-W. Choi, K.-B. Chung, and J.-S. Park, Thin Solid Films **546**, 31-34 (2013)

[20]   C.L. Dezelah, J. Niinisto, K. Arstila, L. Niinisto, and C.H. Winter, Chem. Mater. **18**, 471-475 (2006)

[21]   R.K. Ramachandran, J. Dendooven, J. Botterman, S. Pulinthanathu Sree, D. Poelman, J.A. Martens, H. Poelmand, and C. Detavernier, J. Mater. Chem. A **2**, 19232–19238 (2014)

[22]   R.D. Deslattes, E.G. Kessler Jr, P. Indelicato, and E. Lindroth, International Tables for Crystallography. Vol. C, Section 4.2.2, pp 200-212 (2006)

[23]   P. Moeck, S. Rouvimov, E.F. Rauch, M. Véron, H. Kirmse, I. Häusler, W. Neumann, D. Bultreys, Y. Maniette, and S. Nicolopoulos, Cryst. Res. Technol. **46**, 589-606 (2011)

[24]   www.github.com/pycrystem/pycrystem

[25]   F. de la Peña, T. Ostasevicius, V.T. Fauske, P. Burdet, P. Jokubauskas, M. Nord, M. Sarahan, E. Prestat, D.N. Johnstone, J. Taillon, J. Caron, T. Furnival, K.E. MacArthur, A. Eljarrat, S. Mazzucco, V. Migunov, T. Aarholt, M. Walls, F. Winkler, G. Donval, B. Martineau, A. Garmannslund, L.-F. Zagonel, I. Iyengar, Micrsocopy & Microanalysis **23**, S1, 214-215 (2017)

[26]   S. Fujita, M. Oda, K. Kaneko, and Toshimi Hitora, Jap. J. Appl. Phys. **55**, 1202A3 (2016)

[27]   S.-D. Lee, K. Akaiwa, and S. Fujita, Phys. Status Solidi C **10**, 1592-1595 (2013)

[28]   M. Marezio, and J.P. Remeika, The Journal of Chemical Physics **46**, 1862 (1967)

[29]   F. Rauch, M. Véron, J. Portillo, D. Bultreys, Y. Maniette, and S. Nicolopoulos, Microscopy and Analysis **22**, S5-S8 (2008)

[30]   S. Yoshioka, H. Hayashi, A. Kuwabara, F. Oba, K. Matsunaga, and I. Tanaka, J. Phys.: Condens. Matter **19**, 346211 (2007)

[31]   T. Kawaharamura, G.T. Dang, and M. Furuta. Jap. J. Appl. Phys. **51**, 040207 (2012)

[32]   K. Akaiwa, and S. Fujita, Jap. J. Appl. Phys. **51**, 070203 (2012)